Auracarboranes with and without Au−Au Interactions: An Unusually Strong Aurophilic Interaction

David E. Harwell, Mark D. Mortimer, Carolyn B. Knobler, Frank A. L. Anet, and M. Frederick Hawthorne*

Contribution from the Department of Chemistry and Biochemistry, University of California at Los Angeles, Los Angeles, California 90095-1569

Received November 27, 1995[⊗]

Abstract: The auracarboranes 1,2-$(AuPPh_3)_2$-1,2-$C_2B_{10}H_{10}$ (**1**) and 1,1′-$(AuPPh_3)_2$-[2-(1′,2′-$C_2B_{10}H_{10}$)-1,2-$C_2B_{10}H_{10}$] (**2**) have been synthesized. Both compounds were characterized by NMR and X-ray crystallography. Compound **2** was found to contain an aurophilic interaction between the gold centers. A variable-temperature NMR investigation indicated that the energy barrier separating the gold−gold bonded state and the nonbonded state is 11 ± 1 kcal/mol. Compound **1** crystallized in the monoclinic space group $P2_1/c$ with a = 18.3380(9) Å, b = 14.1037(6) Å, c = 19.4716(8) Å, β = 112.003(2)°, V = 4669 Å^3, and Z = 4. Data were collected using Mo Kα radiation, to a maximum 2θ = 50°, giving 8865 unique reflections, and the structure was solved by heavy atom methods. The final discrepancy index was R = 0.047, R_w = 0.055 for 3423 independent reflections with $I > 3\sigma(I)$. Compound **2** crystallized in the monoclinic space group $P2_1/c$ with a = 14.058(6) Å, b = 18.365(8) Å, c = 20.387(9) Å, β = 109.22(1)°, V = 4970 Å^3, and Z = 4. Data were collected using Mo Kα radiation, to a maximum 2θ = 45°, giving 5232 unique reflections, and the structure was solved by heavy atom methods. The final discrepancy index was R = 0.066, R_w = 0.069 for 2536 independent reflections with $I > 3\sigma(I)$.

Introduction

Although examples of *closo*-carboranes bonded to gold by 2c−2e σ-bonds are relatively rare[1−3] (as opposed to the more widely studied *nido*-carboranes interacting with gold *via* cluster bonding[4−8]), it is known that *ortho*-carborane derivatives form unusually strong Au−C σ-bonds. Mitchell and Stone report that the Au−C bond is unusually stable in the compound 1-Ph_3-PAu-2-Me-1,2-*closo*-$C_2B_{10}H_{10}$, which when reacted with bromine yields the gold(III) complex 1-$Ph_3PAu(Br)_2$-2-Me-1,2-*closo*-$C_2B_{10}H_{10}$ (Scheme 1). Since the reaction of gold alkyls with bromine most often results in cleavage of the Au−C bond, this unusual stability was attributed to the electron-withdrawing influence of the carboranyl cage.[1] Similar stability is seen in σ-bonded gold−perfluoroalkyl compounds.[9,10]

More recent work by Baukova and by Welch reports the synthesis and structural characterization of two related compounds, 1-Ph_3PAu-1,2-*closo*-$C_2B_{10}H_{11}$[3] and 1-CH_3OCH_2-2-Ph_3-PAu-1,2-*closo*-$C_2B_{10}H_{10}$.[2] In both of these species, the Au−C bond is observed to be only 2.039(8) Å. In a theoretical and crystallographic study of model gold−alkyl compounds, Welch observes that this bond is shorter, and consequently stronger, than other gold−carbon σ-bonds, thereby supporting Stone's observations. However, it is Welch's belief that the shortness of the Au−C bond is due to efficient *σ-donor* properties of the carborane and that the carborane does not function as an electron-withdrawing group. None of the gold derivatives described above displayed gold−gold bonding interactions.

Scheme 1

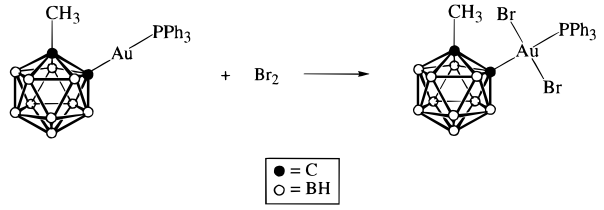

Scheme 2

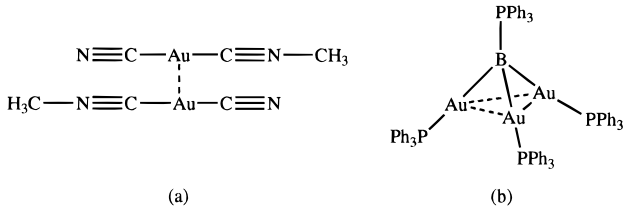

Aurophilicity is defined by Schmidbaur as "the unprecedented affinity between gold atoms even with 'closed-shell' electronic configurations and equivalent electrical charges." Many examples of this phenomenon, including both intermolecular and intramolecular complexes, have now been documented. Representative examples of intermolecular and intramolecular complexes are shown in Scheme 2, parts a and b, respectively.[11,12] The interatomic distance usually observed in these aurophilic interactions is on the order of 3.00 ± 0.25 Å,[13] and their strength has been estimated to be in the range of 6 to 8 kcal/mol.[14−16] Our intention was to ascertain what effect, if

[⊗] Abstract published in *Advance ACS Abstracts,* March 1, 1996.

(1) Mitchell, C. M.; Stone, F. G. A. *Chem. Commun.* **1970**, 1263−1264.
(2) Reid, B. D.; Welch, A. J. *J. Organomet. Chem.* **1992**, *438*, 371−384.
(3) Baukova, T. V.; Kuz'mina, L. G.; Dvortsova, N. V.; Porai-Koshits, M. A.; Kravtsov, D. N.; Perevalova, E. G. *Metalloorg. Khim.* **1989**, *2*, 1098−1105.
(4) Howard, J. A. K.; Jeffery, J. C.; Jelliss, P. A.; Sommerfeld, T.; Stone, F. G. A. *J. Chem. Soc., Chem. Commun.* **1991**, 1664−1666.
(5) Jeffery, J. C.; Jelliss, P. A.; Stone, F. G. A. *J. Chem. Soc., Dalton Trans.* **1993**, 1073−1081.
(6) Jeffery, J. C.; Jelliss, P. A.; Stone, F. G. A. *Inorg. Chem.* **1993**, *32*, 3943−3947.
(7) Jeffery, J. C.; Jelliss, P. A.; Stone, F. G. A. *Organometallics* **1994**, *13*, 2651−2661.
(8) Jeffery, J. C.; Jelliss, P. A.; Stone, F. G. A. *J. Chem. Soc., Dalton Trans.* **1994**, 25−32.
(9) Vaughan, L. G.; Shepard, W. A. *J. Am. Chem. Soc.* **1969**, *91*, 6151−6156.
(10) Nyholm, R. S.; Royo, P. *Chem. Commun.* **1969**, 421.
(11) Blumenthal, A.; Beruda, H.; Schmidbaur, H. *J. Chem. Soc., Chem. Commun.* **1993**, 1005−1006.
(12) Esperas, S. *Acta Chem. Scand.* **1976**, *A30*, 527.
(13) Schmidbaur, H. *Gold Bull.* **1990**, *23*, 11−21.

0002-7863/96/1518-2679$12.00/0

Scheme 3

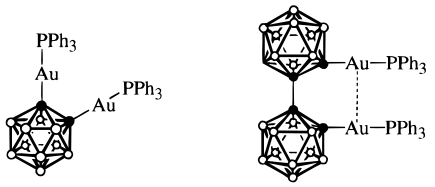

1 **2**

any, the substitution of a carboranyl cage with its unique electronic properties would have upon the physical characteristics of the aurophilic interaction. Consequently, the compound 1,2-$(Ph_3PAu)_2$-1,2-*closo*-$C_2B_{10}H_{10}$ (**1**, Scheme 3) was synthesized. Because the two gold centers of **1** are in close proximity to each other on the carboranyl cage surface we predicted that an aurophilic interaction might be observed. However, the two gold atoms in **1** are restrained by the scaffolding of the carborane cage in positions too far apart to allow interaction. With this in mind, a second system was designed utilizing the free-rotor property of bis(*ortho*-carborane), 1,1′-$(AuPPh_3)_2$-[2-(1′,2′-$C_2B_{10}H_{10}$)-1,2-$C_2B_{10}H_{10}$] (**2**, Scheme 3). Compound **2** is observed to support an aurophilic interaction and the strength of this interaction has been estimated using variable temperature ^{31}P NMR and simulations.

Experimental Section

Materials and Methods. (Triphenylphosphine)gold(I) chloride[17,18] and bis(*ortho*-carborane)[19] were prepared according to literature methods. Standard glovebox, Schlenk, and vacuum line techniques were employed for all manipulations of air- and moisture-sensitive compounds. Reaction solvents were reagent grade and were distilled from appropriate drying agents under nitrogen prior to use. Tetrahydrofuran (THF) was distilled from sodium benzophenone ketyl. Deuterated solvents were obtained from Cambridge Isotope Laboratories Inc., Knoxville, TN. Consumer Health Research of Los Angeles provided *ortho*-carborane. Other reagent grade starting materials were obtained from Aldrich and used without further purification.

Proton (^1H NMR) spectra were obtained with a Bruker AF 200 spectrometer at 200.133 MHz. Carbon (^{13}C NMR) and phosphorus (^{31}P NMR) spectra were obtained using a Bruker AM 400 spectrometer at 100.625 and 161.976 MHz, respectively. Boron (^{11}B NMR) spectra were obtained at 160.46 MHz with a Bruker AM 500 spectrometer. Chemical shifts for ^1H and ^{13}C NMR spectra were referenced to an internal standard of $SiMe_4$ (0.00 ppm) and measured with respect to residual protons in deuterated solvents. Chemical shift values for ^{11}B spectra were referenced relative to external $BF_3{\cdot}OEt_2$ (0.00 ppm). Chemical shift values for ^{31}P spectra were referenced relative to an internal standard of Ph_3PAuCl (33.15 ppm) which was calibrated against an external standard of $P(OMe)_3$ (141.00 ppm). Temperature calibration for variable-temperature NMR measurements was obtained by comparison of $\Delta\delta$ values for methanol below 300 K and $\Delta\delta$ values for ethylene glycol above 300 K.[20] Positive ion FAB mass spectra were obtained from the UCLA Mass Spectrometry Facility at the University of California, Los Angeles.

Synthesis of 1,2-$(AuPPh_3)_2$-1,2-$C_2B_{10}H_{10}$ (1). *ortho*-Carborane (0.20 g, 1.4 mmol) was dissolved in THF (15 mL) and a 2.0 M solution of *n*-butyllithium in hexanes (1.39 mL, 2.78 mmol) was added at 0 °C. The solution was warmed to room temperature and stirred for 2.5 h to form 1,2-Li_2-1,2-$C_2B_{10}H_{10}$. To this solution was added (triphenylphosphine)gold(I) chloride (1.37 g, 2.78 mmol). After stirring at room temperature for an additional 16 h, solvent was removed *in vacuo* and the residue taken up in CH_2Cl_2 (50 mL). The solution was filtered to remove lithium chloride and reduced in volume to *ca*. 10 mL, and 1,2-$(AuPPh_3)_2$-1,2-$C_2B_{10}H_{10}$ was precipitated by addition of diethyl ether (0.83 g, 57%). ^1H NMR ($CDCl_3$) 7.15−7.39 (m, 30 H, C_6H_5) ppm; $^{13}C\{^1H\}$ NMR ($CDCl_3$) 134.2 (C^2, Ph), 131.4 (C^4, Ph), 129.7 (C^1, Ph), 129.0 (C^3, Ph) (CAu not observed due to extreme broadening) ppm; $^{11}B\{^1H\}$ NMR (acetone) −1.8 (2 B), −7.1 (2 B), −9.1 (6 B) ppm; $^{31}P\{^1H\}$ NMR ($CDCl_3$) 38.5 ppm. High resolution positive ion FAB mass spectroscopy calculated mass for $C_{38}H_{40}{}^{10}B_1{}^{11}B_9Au_2P_2$ *m/z* 1061.2930; observed *m/z* 1061.2924.

Synthesis of 1,1′-$(AuPPh_3)_2$-[2-(1′,2′-$C_2B_{10}H_{10}$)-1,2-$C_2B_{10}H_{10}$] (2). Bis(*ortho*-carborane), (0.27 g, 0.94 mmol) was dissolved in THF (100 mL) and a 2.5 M solution of *n*-butyllithium in hexanes (0.75 mL, 1.9 mmol) was added. The solution was stirred for 0.5 h to form 1,1′-Li_2-[2-(1′,2′-$C_2B_{10}H_{10}$)-1,2-$C_2B_{10}H_{10}$]. To this solution was added (triphenylphosphine)gold(I) chloride (0.933 g, 1.89 mmol). The reaction flask was then fitted with a condenser and the solution was heated at reflux for 3 h. After stirring at room temperature for an additional 12 h, solvent was removed *in vacuo* and the residue taken up in CH_2Cl_2 (50 mL). The solution was filtered to remove lithium chloride and reduced in volume to *ca*. 10 mL, and 1,1′-$(Ph_3PAu)_2$-[2-(1′,2′-$C_2B_{10}H_{10}$)-1,2-$C_2B_{10}H_{10}$] was isolated using column chromatography (alumina, 3% CH_3OH: 97% CH_2Cl_2) (0.67 g, 59%). ^1H NMR ($CDCl_3$) 7.36−7.63 (m, 30 H, C_6H_5), 0.7−3.3 (vbr, 10 H BH) ppm; $^{13}C\{^1H\}$ NMR ($CDCl_3$) 134.0 (C^3, Ph), 131.6 (C^1, Ph), 129.3 (C^4, Ph), 129.2 (C^2, Ph) (CAu not observed due to extreme broadening) ppm; $^{11}B\{^1H\}$ NMR (acetone) −2.3 (4 B), −7.6 (14 B), −12.6 (2 B) ppm; $^{31}P\{^1H\}$ NMR ($CDCl_3$) 36.8 ppm. High resolution positive ion FAB mass spectroscopy calculated mass for $C_{40}H_{50}{}^{10}B_8{}^{11}B_{12}Au_2P_2$ *m/z* 1203.4717; observed *m/z* 1203.4717.

Crystal Structure Determinations. Computer programs used in the crystal structure determinations include locally modified versions of the following programs: CARESS (Broach, Coppens, Becker, and Blessing), peak profile analysis, Lorentz and polarization correction, and full-matrix least-squares refinement; ABSCOR, absorption correction based on psiscans; SHELX76 (Sheldrick), a crystal structure package; SHELX86 (Sheldrick), a crystal structure package; and ORTEP (Johnson). X-ray data were collected on a Huber diffractometer constructed by Professor C. E. Strouse of this department. Data were collected at 25 °C in the $\theta-2\theta$ scan mode and were corrected for Lorentz and polarization effects and for secondary extinction and absorption. Atoms were located by use of heavy atom methods. All calculations were performed on a VAX 3100 computer in the J. D. McCullough X-Ray Crystallography Laboratory. Gold and phosphorus atoms were refined with anisotropic parameters. Phenyl rings were refined as rigid C_6H_5 groups: C−C 1.395 Å, C−H 1.0 Å, angles 120°. Other hydrogen atoms were included in located positions. H atoms were assigned isotropic displacement values based approximately on the value for the attached atom. Scattering factors for H were obtained from Stewart *et al.*[21] and for other atoms were taken from the *International Tables for X-Ray Crystallography*.[22]

Data Collection and Structure Refinement of 1. A yellow crystal, obtained from a pentane/THF solution, was mounted on a glass fiber. Unit cell parameters were determined from a least-squares fit of 89 accurately centered reflections ($7.6 < 2\theta < 20.1°$). These dimensions and other parameters, including conditions of data collection, are summarized in Table 1. Three intense reflections (3,−2,0; 3,2,0; 1,0,4) were monitored every 97 reflections to check stability. Intensities of these reflections did not decay during the course of the experiment (79.8 h). Of these 5595 unique reflections measured, 3423 were considered observed ($I > 3\sigma(I)$) and were used in the subsequent structure analysis. A molecule of THF has been included as five carbon atoms and no hydrogen atoms were included for this solvent molecule. The largest peak on a final difference electron density map, near Au(1), was 0.55 e $Å^{-3}$.

(14) Dziwok, K.; Lachmann, J.; Wilkinson, D. L.; Müller, G.; Schmidbaur, H. *Chem. Ber.* **1990**, *123*, 423−431.
(15) Schmidbaur, H.; Graf, W.; Müller, G. *Angew. Chem., Int. Ed. Engl.* **1988**, *27*, 417−421.
(16) Schmidbaur, H.; Graf, W.; Müller, G. *Helv. Chim. Acta* **1986**, *69*, 1748−1756.
(17) McAuliffe, C. A.; Panish, R. V.; Randall, P. D. *J. Chem. Soc., Dalton Trans.* **1979**, *1979*, 1730.
(18) Bruce, M. I.; Nicholson, B. K.; Shawkataly, O. B. *Inorg. Synth.* **1989**, *26*, 324.
(19) Paxson, T. E.; Callahan, K. P.; Hawthorne, M. F. *Inorg. Chem.* **1973**, *12*, 708−709.
(20) *Variable Temperature Unit B-VT 2000 Manual*; USA Bruker Instrument Inc.
(21) Stewart, R. F.; Davidson, E. R.; Simpson, W. T. *J. Chem. Phys.* **1965**, *42*, 3175.
(22) *International Tables for X-ray Crystallography*; Kynoch Press: Birmingham, England, 1974; Vol. IV.

Table 1. Details of Crystallographic Data Collection for Compounds **1** and **2**

parameter	**1**	**2**
formula	$C_{38}H_{40}B_{10}Au_2P_2$	$C_{40}H_{50}B_{20}Au_2P_2$
formula weight	1061	1202
temperature (°C)	25	25
crystal size (mm)	0.08 × 0.2 × 0.4	0.05 × 0.05 × 0.3
normal to faces	100, 010, 001	001, 010, $\bar{1}$01
appearance	yellow plate	pale yellow needle
radiation (graphite monochromator)	Mo Kα	Mo Kα
wavelength (Å)	0.7107	0.7107
space group	$P2_1/c$	$P2_1/c$
a (Å)	18.3380(9)	14.056(6)
b (Å)	14.1037(6)	18.365(8)
c (Å)	19.4716(38)	20.387(9)
β (deg)	112.003(2)	109.22(1)
V (Å^3)	4669	4970
Z	4	4
density (g cm^{-3}), calcd	1.61	1.66
μ (cm^{-1})	63.6	60.3
scan width, below Kα_1	1.3	1.3
scan width, above Kα_2	1.6	1.6
scan rate (deg min^{-1})	6.	3.
no. of unique reflcns	5595	5232
no. of obsd ($I > 3\sigma(I)$) reflcns	3423	2536
2θ max (deg)	50	45
data collected	$+h,+k,\pm l$	$+h,+k,\pm l$
no. of parameters refined	178	222
R	0.047	0.066
R_w	0.055	0.069
GOF	1.51	1.55

Data Collection and Structure Refinement of 2. A pale yellow crystal, obtained from a pentane/CH_2Cl_2 solution, was mounted on a fiber. Unit cell parameters were determined from a least-squares fit of 20 accurately centered reflections ($7.3 < 2\theta < 16.2°$). These dimensions and other parameters, including conditions of data collection, are summarized in Table 1. Three intense reflections (0,4,0; 1,0,4; 5,2,−1) were monitored every 97 reflections to check stability. Intensities of these reflections decayed 6% during the course of the experiment (128.9 h). Of the 5232 unique reflections measured, 2536 were considered observed ($I > 3\sigma(I)$) and were used in the subsequent structure analysis. A molecule of CH_2Cl_2 was included as one carbon atom and three chlorine atoms all at $^1/_4$ occupancy. This solvent molecule must be disordered because it was found to lie near a center of inversion. The largest peak on a final difference electron density map, near Au(1), was 0.5 e Å^{-3}.

Results and Discussion

Synthesis of 1 and 2. Compounds **1** and **2** were prepared by a method similar to that reported by Mitchell and Stone for the synthesis of compounds containing a single Au−C σ-bond.[1] Reaction of either *ortho*-carborane or bis(*ortho*-carborane) with 2 molar equiv of *n*-butyllithium afforded the respective dilithium salt, which when reacted with 2 molar equiv of (triphenylphosphine)gold(I) chloride gave the diauracarborane species in 57% (**1**) and 59% (**2**) yields (Scheme 4).

Compounds **1** and **2** are yellow crystalline materials which are readily soluble in THF, acetone, chloroform, and dichloromethane. Both compounds are air-stable; however, **2** was observed to slowly decompose in solution.

X-ray Structural Analysis of 1. An ORTEP representation of **1** is presented in Figure 1 and important bond lengths and angles appear in Table 2. The carboranyl cage of **1** is found to be a regular icosahedron with gold(triphenylphosphine) groups bonded perpendicularly to the icosohedral surface at the two carbon vertices. The interatomic angles B(12)−C(1)−Au(1) and B(9)−C(2)−Au(2) are 174.0(8)° and 176.3(7)°, respectively. Bond angles around the gold atoms are also nearly linear with angles of 178.9(4)° and 174.2(4)° for P(1)−Au(1)−C(1) and P(2)−Au(2)−C(2), respectively. These values agree well with those reported for Au(I) centers in similar compounds.[11,15,23,24] The lack of distortion around the gold centers coupled with the Au(1)−Au(2) distance of 3.567(1) Å, well outside the more usual range of 3.00 ± 0.25 Å,[13] precludes an aurophilic interaction. This is presumably due to the rigidity of the carborane cage, which prevents the gold(triphenylphosphine) substituents from closely approaching each other.

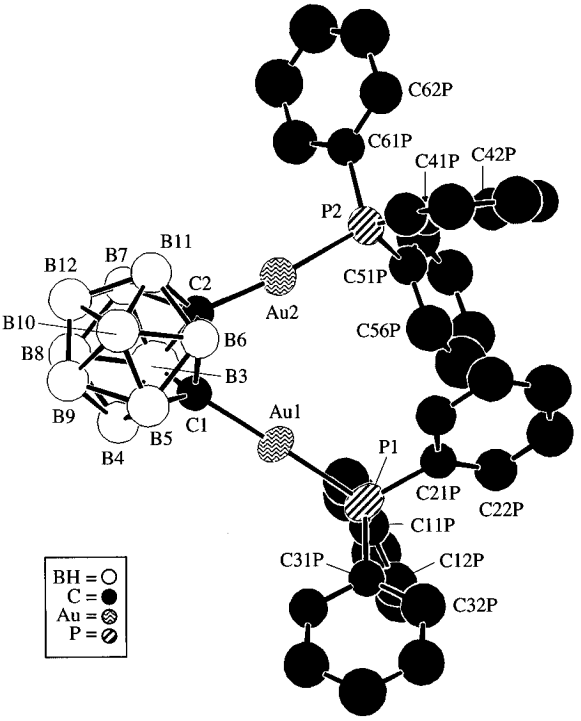

Figure 1. ORTEP representation of compound **1**, 1,2-$(AuPPh_3)_2$-1,2-$C_2B_{10}H_{10}$, showing the numbering scheme. All hydrogens are removed for clarity. Ellipsoids are drawn at the 0.50 probability level.

Scheme 4

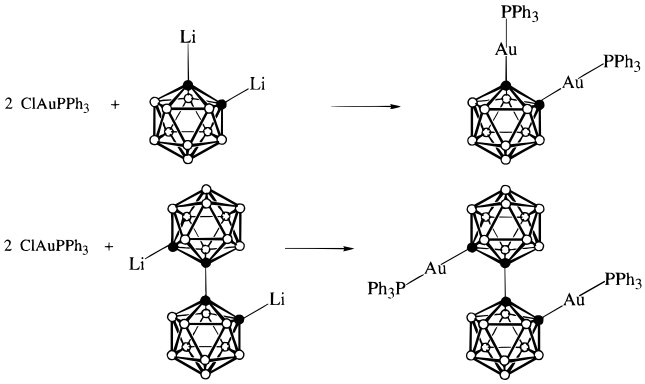

Table 2. Selected Bond Parameters for **1**

bond	distance (Å)	bond	distance (Å)
Au(1)−P(1)	2.270(4)	Au(2)−P(2)	2.273(5)
Au(1)−C(1)	2.055(14)	Au(2)−C(2)	2.033(15)
P(1)−C(31P)	1.807(12)	P(2)−C(41P)	1.794(12)
C(1)−C(2)	1.71(2)	Au(1)−Au(2)	3.567(1)

atoms	angle (deg)	atoms	angle (deg)
P(1)−Au(1)−C(1)	178.9(4)	P(2)−Au(2)−C(2)	174.2(4)
Au(1)−P(1)−C(11P)	112.9(4)	C(11P)−P(1)−C(31P)	104.0(5)
B(12)−C(1)−Au(1)	174.0(8)	B(9)−C(2)−Au(2)	176.3(7)

(23) Schmidbaur, H.; Graf, W.; Müller, G. *Helv. Chim. Acta* **1986**, *69*, 1748−1756.
(24) Crane, V. S.; Beall, H. *Inorg. Chim. Acta* **1978**, *31*, L469-L470.

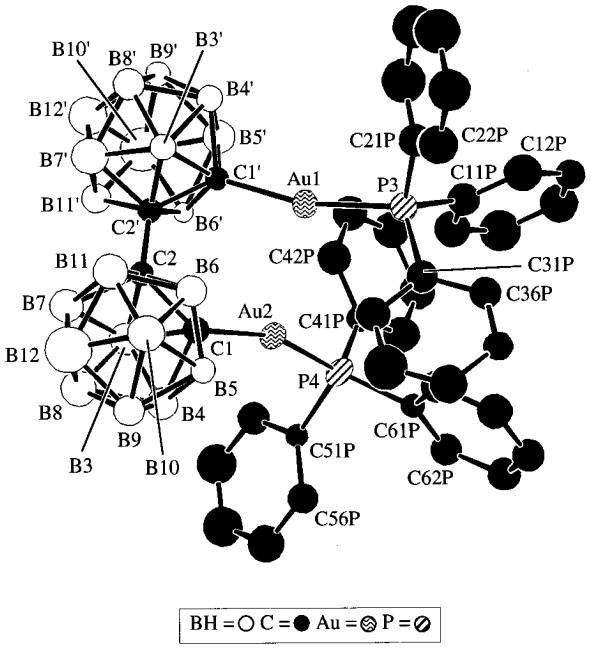

Figure 2. ORTEP representation of compound **2**, 1,1′-$(AuPPh_3)_2$-[2-(1′,2′-$C_2B_{10}H_{10}$)-1,2-$C_2B_{10}H_{10}$], showing the numbering scheme. All hydrogens are removed for clarity. Ellipsoids are drawn at the 0.50 probability level.

Table 3. Selected Bond Parameters for **2**

bond	distance (Å)	bond	distance (Å)
Au(1)−P(3)	2.293(8)	Au(2)−P(4)	2.281(9)
Au(1)−C(1′)	2.09(3)	Au(2)−C(1)	2.13(3)
P(3)−C(11P)	1.82(2)	P(4)−C(41P)	1.82(2)
C(2)−C(2′)	1.51(4)	Au(1)−Au(2)	3.119(2)

atoms	angle (deg)	atoms	angle (deg)
P(3)−Au(1)−C(1′)	166.2(8)	P(4)−Au(2)−C(1)	161.4(8)
Au(1)−P(3)−C(11P)	111.2(8)	C(11P)−P(3)−C(31P)	108.2(10)
Au(2)−P(4)−C(41P)	116.9(7)	C(41P)−P(4)−C(61P)	105.6(10)
Au(2)−C(1)−C(2)	127(2)	Au(2)−C(1)−B(4)	107(2)
Au(2)−C(1)−B(6)	128(2)	B(9′)−C(2′)−C(2)	176(2)
C(2′)−C(2)−B(9)	177(2)	C(2′)−C(1′)−Au(1)	130(2)
C(2)−C(1)−Au(2)	127(2)	B(12)−C(1)−Au(2)	168(1)
B(12′)−C(1′)−Au(1)	170(1)		

atoms	dihedral angle (deg)
C(1)−C(1′)−Au(1)−Au(2)	31(4)
C(1′)−C(2′)−C(2)−C(1)	31(4)
C(2)−C(2′)−Au(1)−Au(2)	49(2)
C(1′)−midpt. C(2)C(2′)−midpt. Au(1)Au(2)−Au(2)	144(1)
C(1)−midpt. C(2)C(2′)−midpt. Au(1)Au(2)−Au(1)	141(1)
C(1′)−midpt. C(1)C(1′)−midpt. Au(1)Au(2)−Au(2)	142
C(1)−midpt. C(1)C(1′)−midpt. Au(1)Au(2)−Au(1)	142

X-ray Structural Analysis of 2. An ORTEP representation of **2** is presented in Figure 2 and important bond lengths and angles appear in Table 3. In the solid state the gold(triphenylphosphine) moieties are both on the same side of the molecule, with an Au(1)−Au(2) distance of 3.119 Å. This is within the range of distances reported for other molecules with an aurophilic interaction,[15,16,23,25,26] and much shorter than that seen in compound **1**. The structure as shown in Figure 2 is chiral, but the space group is $P2_1/c$; therefore, the crystal contains a 1:1 mixture of both enantiomers. A view down the long axis of the bis(*ortho*-carborane) group reveals that the gold atoms of **2** are not eclipsed, but instead are rotated 49(2)° away from each other as defined by the dihedral angle Au(1)−C(2)−C(2′)−Au(2). The angles B(12)−C(1)−Au(2) and B(12′)−C(1′)−Au(1) are 168(1)° and 170(1)°, respectively, showing significant distortions from linearity. Likewise, the bond angles P(3)−Au(1)−C(1′) and P(4)−Au(2)−C(1) are 166.2(8)° and 161.4(8)°, respectively, and nonlinear. Significantly, the gold atoms are displaced *away* from each other, rather than being pulled together by their mutual attraction. This implies that the aurophilic interaction is competing with the mutual steric repulsion arising from the bulky triphenylphosphine ligands. Although distortions have been reported for gold(I) centers in Au-bridging and cluster compounds, the angle of 161.4(8)° observed at the gold center reported here is the largest distortion from linearity reported for a gold−phosphine complex of this coordination type of which we are aware.[11,15,16,23,25−27] The phenyl groups attached to the two phosphorus atoms of **2** are intermeshed in a fashion resembling the cogs of two gears and their component atoms are not within van der Waals radii of each other. The distortions in the structure of **2**, concomitant with the formation of the aurophilic interaction, are in marked contrast to the undistorted structure of compound **1**, which contains no such interaction. All the relief of steric strain associated with the formation of the aurophilic interaction is localized within the gold(triphenylphosphine) groups and their connections to the bis(*ortho*-carborane) moiety. The bis(*ortho*-carborane) itself shows very little distortion from its expected geometry. In particular, the angles B(9)−C(2)−C(2′) and C(2)−C(2′)−B(9′) are 177(2)° and 176(2)°, respectively.

Multinuclear NMR Analysis of 1. Only the resonances due to the phenyl groups associated with the PPh_3 ligands of **1** are observed in the ^1H and $^{13}C\{^1H\}$ NMR spectra. The signals of the hydrogens attached to the boron atoms of a carborane cage are invariably quite broad and are seen for compound **1** as a slight protuberance in the baseline of the ^1H NMR spectrum between 0.70 and 3.30 ppm. Signals arising from the carbons of the carborane cage are not observed, presumably due to line broadening as a result of their direct attachment to borons in the cage and coupling to ^{31}P nuclei. The $^{11}B\{^1H\}$ NMR spectrum of **1** displays three peaks in a ratio of 2:2:6 with chemical shifts of −1.8, −7.1, and −9.6 ppm. The pattern and the shifts observed are consistent with a disubstituted *ortho*-carborane cage. The $^{31}P\{^1H\}$ NMR spectra of **1** exhibits only a single resonance, at 38.5 ppm.

Multinuclear NMR Analysis of 2. The NMR spectra of **2** are very similar to the corresponding spectra of **1**. Again, the resonance expected from the carbons of the carborane cages attached to the gold centers is not observed in the $^{13}C\{^1H\}$ NMR spectrum. Significantly, the observed resonance for compound **2** in the $^{31}P\{^1H\}$ NMR spectrum was broad, whereas the corresponding spectrum of **1** was not, indicating that a dynamic process was occurring on the NMR time scale. A variable-temperature NMR study was therefore undertaken with the objectives of freezing-out the different conformations of **2** and determining the energy barrier for their interconversion.

Variable-Temperature ^{31}P NMR Analysis of 2. The $^{31}P\{^1H\}$ NMR spectrum of compound **2** was measured at roughly 10-deg intervals between 200 and 310 K in $CDCl_3$ (Figure 3a), using the proton chemical shifts of either methanol or ethylene glycol as temperature calibrants. At temperatures of 280 K and above, a major peak is observed which becomes sharper as the temperature is increased. A small subsidiary peak at 37 ppm arises from an unidentified phosphorus-containing impurity. The spectrum taken at 278 K is very close to the coalescence point.

(25) Schmidbaur, H.; Zeller, E.; Weidenhiller, G.; Steigelmann, O.; Beruda, H. *Inorg. Chem.* **1992**, *31*, 2370−2376.
(26) Schmidbaur, H.; Brachthäuser, B.; Steigelmann, O.; Beruda, H. *Chem. Ber.* **1992**, *125*, 2705−2710.
(27) Scherbaum, F.; Huber, B.; Müller, G.; Schmidbaur, H. *Angew. Chem., Int. Ed. Engl.* **1988**, *27*, 1542−1544.

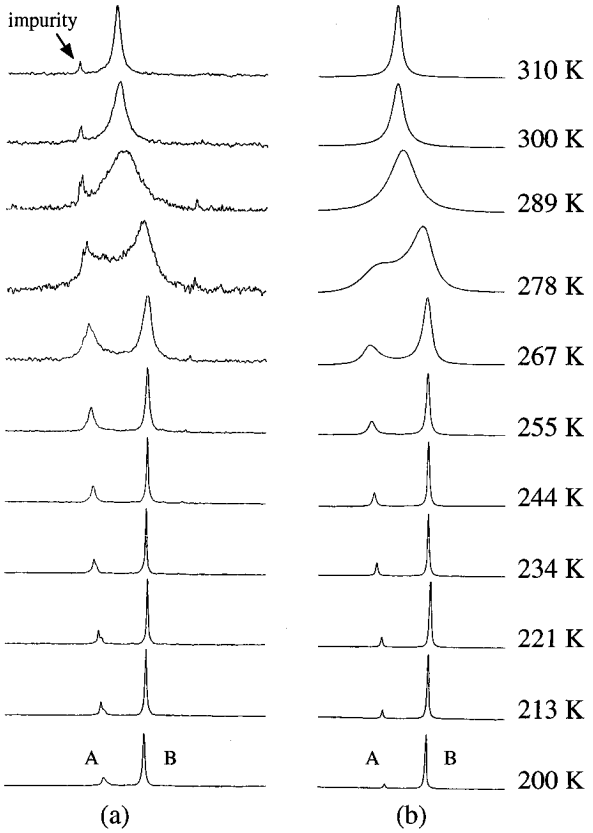

Figure 3. (a) Observed variable-temperature $^{31}P\{^1H\}$ NMR spectra of **2** in deuteriochloroform. (b) Simulated variable-temperature $^{31}P\{^1H\}$ NMR spectra of **2**.

Scheme 5

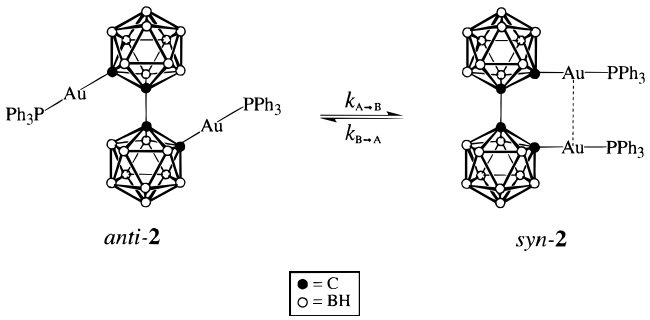

At temperatures below 280 K, two resonances are observed. Only one resonance can be assigned to the structure observed in the X-ray analysis of **2**; however, the second resonance must correspond to a closely related structure and the two structures must be interconverting more or less slowly on the NMR time scale. We ascribe these resonances to the freezing-out of the gold−gold bonded (*syn*) and the non-interactive (*anti*) conformations of **2** as depicted in Scheme 5. The chemical shift of one peak (A) is strongly temperature dependent, although the temperature dependence of peak B is minimal in the temperature range studied. The relative populations of the two peaks vary greatly. At 200 K, peak B (90%) is extensively more populated than peak A (10%), whereas above room temperature peak A (55 %) is more populated than peak B (45%), as shown by the dynamic NMR study presented below. These observations indicate that peak B corresponds to the enthalpically favored conformation whereas peak A corresponds to the entropically favored conformation. Therefore, we assigned *anti*-**2**, the species with the larger entropy (more rotational states), to peak A, and *syn*-**2**, the rigid species observed in the crystal structure, to peak B.

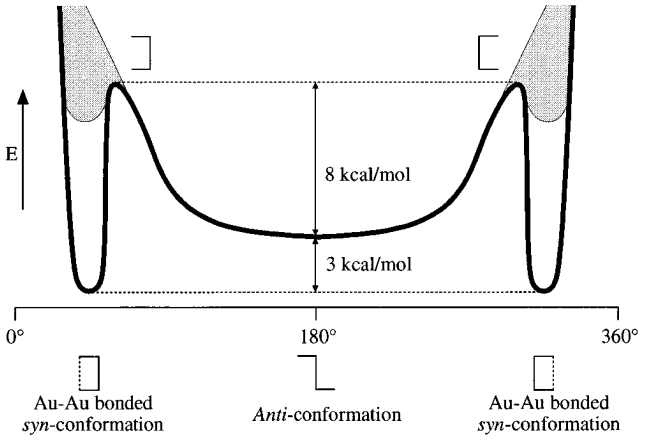

Figure 4. Proposed potential energy diagram for the interconversion of *syn*-**2** and *anti*-**2**. For an explanation see text.

The Nature of the Energy Barrier to Interconversion. Figure 4 is a diagram depicting the potential energy of **2** with respect to rotation around the C(2)−C(2′) axis (bold line). In solution **2** exists in one of two conformations, *anti*-**2** or *syn*-**2** (Scheme 5). Both of the mirror image structures of *syn*-**2** are possible, and the crystal structure of **2** is observed to consist of a 1:1 mixture of the two enantiomers. The crystal structure represents the lowest energy (*syn*) conformation of **2** in the solid state, and corresponds to the two deep wells on each side of the energy diagram (one for each of the enantiomers). The center well of the energy diagram is broad and corresponds to the several different configurations of similar energy possible for the *anti*-conformation of **2**, which are related to one another by rotation around the C(2)−C(2′) axis. As the Ph_3PAu groups are brought into closer proximity to each other by rotation about the C(2)−C(2′) axis the energy is expected to rise due to steric repulsions until the gold atoms become sufficiently close for a bonding interaction to occur. Formation of the aurophilic interaction would then result in a lowering of the energy which is depicted by the narrow wells on each side of Figure 4.

Large energy barriers are depicted on the extreme left and right sides of Figure 4 to indicate that there is no interconversion between enantiomers by the (triphenylphosphine)gold groups rotating past each other. The X-ray structure of **2** suggests that such a rotation is highly unlikely. In fact, the manner in which the gold atoms are bent away from each other by the steric bulk of the attached phosphine groups implies that the molecule is already under considerable steric strain. Narrow wells are indicated for the *syn*-conformations of **2** because the X-ray structure of **2** indicates that the aurophilic interaction is at a maximum when the dihedral angle Au(1)−C(2)−C(2′)−Au(2) is 49°. Angles less than 49° would result in excessive steric strain which could not be compensated by the increase in gold−gold orbital overlap. Angles much greater than 49° would result in rotating the gold atoms too far apart to maintain the aurophilic interaction.

We have calculated a value for the barrier between *anti*-**2** and *syn*-**2** (*vide infra*); however, the energy of the aurophilic interaction does not necessarily correspond to this value. In reference to Figure 4, the energy of the aurophilic interaction is measured vertically from the bottom of either of the narrow wells representing *syn*-**2** up to the surface of the potential energy plot for **2** in the *absence* of an aurophilic interaction. (The transition state at the top of the energy barrier will have a certain amount of gold−gold bonding character.) Two possibilities exist for the potential energy of **2** in the absence of an aurophilic interaction. At one extreme, the potential energy would increase rapidly on each side of a broad minimum asthe two Ph_3PAu

Table 4. Calculated Parameters for Simulated ^{31}P NMR Spectra of **2**

temp (K)	$\Delta G^{\circ}_{A\rightarrow B}$ (kcal/mol)	$\Delta G^{\ddagger}_{A\rightarrow B}$ (kcal/mol)	$k_{A\rightarrow B}$ (s^{-1})	δ_A (ppm)	δ_B (ppm)	$\Delta\nu$ (Hz)	P_A
200	1.01	11.0	4.0	36.9	36.5	69	0.07
213	0.88	11.2	1.4×10^1	37.0	36.5	77	0.11
221	0.80	11.3	3.0×10^1	37.0	36.5	81	0.14
234	0.68	11.5	8.5×10^1	37.0	36.5	87	0.19
244	0.58	11.7	1.8×10^2	37.1	36.5	92	0.23
255	0.47	11.8	3.7×10^2	37.1	36.5	97	0.28
267	0.35	12.0	7.8×10^2	37.1	36.5	103	0.34
278	0.25	12.2	1.5×10^3	37.2	36.5	108	0.39
289	0.13	12.4	2.6×10^3	37.2	36.5	113	0.44
300	0.03	12.6	4.5×10^3	37.2	36.5	119	0.49
310	−0.07	12.7	7.1×10^3	37.3	36.5	123	0.53

groups are rotated into one another. This extreme is depicted by the fine lines across the top of the gray areas in Figure 4. The other extreme, depicted by the fine lines at the bottom of the gray areas in Figure 4, arises from possible energy-lowering interactions between the phosphine groups upon close contact. These might include, for example, a local energy minimum as the phenyl goups on the phosphorus atoms intermesh, or attractive edge face or π-stacking interactions. The actual potential energy surface for **2** in the absence of the aurophilic interaction most likely lies somewhere between these two extremes within the gray areas, and thus the energy of the interaction may be somewhat stronger or weaker than the height of the barrier from *syn*-**2** to *anti*-**2**. The calculation of this barrier will be discussed in the next section. It should be noted that the ambiguity in the assignment of a value for the energy of the aurophilic interaction should not be confused with the error in the calculation of the barrier to interconversion between *anti*-**2** and *syn*-**2**. The calculation of this error will also be discussed later in the paper.

^{31}P NMR Simulations. Simulated spectra were calculated using the equations of Rogers and Woodbrey,[28] and the final values of the important parameters are given in Table 4. P_A is defined as the fractional population of *anti*-**2**, corresponding to the area under peak A in the spectra, and P_B ($=1 - P_A$) is defined as the fractional population of *syn*-**2**, corresponding to the area under peak B in the spectra (Figure 3a). The rate constants $k_{A\rightarrow B}$ and $k_{B\rightarrow A}$ are defined as the rate of conversion of *anti*-**2** to *syn*-**2** and the reverse, respectively. The time τ is defined by eq 1, and $\Delta\nu$ is the difference in the chemical shifts of peaks A and B expressed in hertz.

$$\tau = (k_{A\rightarrow B} + k_{B\rightarrow A})^{-1} \tag{1}$$

The spectral line shape depends on P_A, τ, $\Delta\nu$, and the T_2 values of A and B in the absence of exchange. Values of T_2, the transverse (spin−spin) relaxation time, for *anti*-**2** and *syn*-**2** were estimated by measuring the width at half-height of the peaks A and B, respectively, in the slow-exchange region (213 K) and these values were held constant in all calculations. Initial values for P_A and P_B were determined by integrating peaks A and B at each temperature and then systematically subtracting the contribution due to the small impurity at 37 ppm. The contribution due to the impurity was determined by integration in the fast-exchange region where the combined peak for A and B was well differentiated from the impurity peak. Calculated spectra were fitted to the experimental spectra by changing the values of τ and the ratio of P_A to P_B. Values for the thermodynamic parameter ΔG° were then calculated utilizing eq 2 at each temperature and plotted against temperature, where $K_1 = P_A/P_B$. Utilizing the linear relationship of ΔG° with respect to temperature (eq 3a), a least-squares analysis was used to obtain a best-fit straight line, and values for P_A and P_B were optimized based on the best fit. The improved values for P_A and P_B were used to obtain new values for τ. Values for the kinetic parameter $\Delta G^{\ddagger}$ were calculated from the newly obtained values for τ utilizing the Eyring equation (eq 4)[29,30] where **k**

$$\Delta G^{\circ} = -RT \ln K_1 \tag{2}$$

$$\Delta G^{\circ} = \Delta H^{\circ} - T\Delta S^{\circ} \tag{3a}$$

$$\Delta G^{\ddagger} = \Delta H^{\ddagger} - T\Delta S^{\ddagger} \tag{3b}$$

$$\Delta G^{\ddagger} = -RT \ln \left(\frac{kh}{\mathbf{k}T}\right) \tag{4}$$

represents the Boltzmann constant, and plotted against temperature. A least-squares analysis was again performed to obtain a straight line. The equations for both plots (ΔG° vs T and $\Delta G^{\ddagger}$ vs T) were entered into a spreadsheet and the values of their gradients (ΔS° and $\Delta S^{\ddagger}$, respectively) and y-intercepts (ΔH° and $\Delta H^{\ddagger}$, respectively) were varied in an iterative process until the best fit for all data points was obtained (Figure 3b, Table 4).

Evaluation of Error in NMR Calculations. Values for ΔG are related to the values of ΔH and ΔS through the Gibbs function (eqs 3a and 3b). Insertion of the constant T_M, which represents the mean temperature of the experimental measurements, results in eq 5. The constant, ΔG_M, can be defined as the value for ΔG at T_M, and $T - T_M$ can be rewritten as ΔT. Therefore, eq 5 can be simplified to eq 6. Insertion of the variable $\Delta\Delta S$, which is defined as the change in ΔS, yields eq 7.

$$\Delta G = \Delta H - T_M\Delta S - (T - T_M)\Delta S \tag{5}$$

$$\Delta G = \Delta G_M - \Delta T\Delta S \tag{6}$$

$$\Delta G = \Delta G_M - \Delta T(\Delta S + \Delta\Delta S) \tag{7}$$

Values for $\Delta\Delta S$ were varied incrementally and new values for ΔG° and $\Delta G^{\ddagger}$ were calculated. Values for τ and the ratio of P_A to P_B were calculated from ΔG° and $\Delta G^{\ddagger}$, respectively. These newly obtained values were used to calculate a set of simulated spectra. The value of $\Delta\Delta S$ was changed until the simulated spectra were judged to no longer agree with the observed spectra. The minimum values of $\Delta\Delta S^{\circ}$ and $\Delta\Delta S^{\ddagger}$ where the calculated spectra no longer fit the observed spectra were taken as the error in ΔS° and $\Delta S^{\ddagger}$, respectively. The error in ΔH° and $\Delta H^{\ddagger}$ can be calculated by the relationship depicted in eq 8 where $\Delta\Delta H$ is defined as the change in ΔH (Table 5).

$$\Delta\Delta H = T\Delta\Delta S \tag{8}$$

Table 5. Ground State and Activation Parameters for **2**

$\Delta H^{\circ}_{A\rightarrow B}$ (kcal/mol)	$\Delta S^{\circ}_{A\rightarrow B}$ (eu)	$\Delta H^{\ddagger}_{A\rightarrow B}$ (kcal/mol)	$\Delta S^{\ddagger}_{A\rightarrow B}$ (eu)	$\Delta H^{\ddagger}_{B\rightarrow A}$ (kcal/mol)	$\Delta S^{\ddagger}_{B\rightarrow A}$ (eu)
3.0 ± 0.5	10 ± 2	11 ± 1	6 ± 3	8 ± 1	-8 ± 3

Table 5 shows the final calculated values for the entropies and enthalpies of transition, and for the process as a whole. The *syn*-conformation of **2** was found to be 3 ± 0.5 kcal/mol more stable than the *anti*-conformation (Figure 4), with the added stability of *syn*-**2** attributed to the aurophilic interaction. The height of the energy barrier going from the *anti*-conforma-

(28) Rogers, M. T.; Woodbrey, J. C. *J. Phys. Chem.* **1962**, *66*, 540−546.

(29) Glasstone, S.; Laidler, K. J.; Eyring, H. *The Theory of Rate Processes*; McGraw-Hill: New York, 1941.

(30) Eyring, H. *Chem. Rev.* **1935**, *17*, 65.

tion to the transition state was calculated as 8 ± 1 kcal/mol, while the height going from the *syn*-conformation to the transition state was calculated as 11 ± 1 kcal/mol. In physical terms, the *anti* to transition state barrier represents the significant structural distortions discussed in the X-ray structural analysis. Potential energy is bound up in the deviation of the angles around gold and the carbons attached to gold from their optimal hybridization in the absence of the aurophilic interaction. The *syn* to transition state barrier represents the energy required to break the aurophilic interaction, plus any energy which may be associated with disentangling the phosphine groups. However, this is anticipated to be a minor term and we feel justified in using the figure of 11 ± 1 kcal/mol as a good estimate of the strength of the aurophilic interaction.

The value of 11 ± 1 kcal/mol for the aurophilic interaction is approximately one and a half times that previously estimated in other systems at between 6 and 8 kcal/mol.[14,15,23] We believe that the explanation for this surprisingly strong interaction is to be found in the powerful electron-withdrawing nature of the *ortho*-carboranyl groups, which make the gold atoms more electron deficient than in other gold(I) compounds. This is compensated for by maximizing bonding interactions between the gold atoms. In this we agree with Stone's interpretation of the nature of the carboranyl group as an electron-withdrawing substituent and disagree with Welch's alternative view that it acts as an electron donor. A great deal of independent study over the past 30 years has led to the characterization of a C-*ortho*-carboranyl group as powerfully electron-withdrawing (as opposed to B-*ortho*-carboranyl groups which are more or less electron-donating, depending on the position of B-substitution). Arguments are based on the high acid strength of carboranyl carboxylic acids,[31−34] Hammett σ-constant determinations[35] and Taft analysis of ^{19}F NMR shifts[32,36,37] of suitable derivatives, the ease of metalation of the carboranyl C−H group,[38,39] the relative lack of reactivity of C-halomethyl carboranes toward nucleophiles,[1,40,41] and a host of other observations regarding the reactivity of these species.[42−54]

In addition to the electron-withdrawing ability of the carboranyl cage, we believe that the shortening of the Au−C bond length observed by Stone, Baukova, and Welch is due to the hybridization of the atomic orbitals of the carbon in the carborane cage. This hybridization has more s-character than traditional alkyl, sp^3, substituents. Consequently bonds involving C-vertices of carborane should be shorter and, in fact, C−C bonds between the carbon of a carboranyl-cage and an alkyl substituent are observed to be shorter than C−C bonds in alkanes.[55]

Conclusions

We have succeeded in synthesizing both a gold−carborane compound containing an aurophilic interaction and an electronically similar model compound having no aurophilic interaction for comparison. Detailed NMR variable-temperature experiments coupled with crystallographic analyses have allowed us to propose an explanation of the fluxional behavior of **2** based on a dynamic equilibrium between the *syn* and *anti* forms of the compound, and to estimate the strength of the aurophilic interaction based on the calculated height of the barrier to interconversion. The strength of this interaction, at 11 kcal/mol, is considerably greater than that previously estimated by Schmidbaur et al. using similar techniques. We propose that the electron-deficiency of the gold atoms caused by the strong negative inductive effect of the carborane cages is responsible for the stronger interaction, in contradiction to other analyses of the nature of gold carboranyl compounds.

Acknowledgment. We thank the National Science Foundation for their financial support of this work under Grant No. NSF-CHE-93-14037.

Supporting Information Available: Tables of bond distances and angles and position and displacement parameters (13 pages); listing of observed and calculated structure factors for **1** and **2** (35 pages). This material is contained in libraries on microfiche, immediately follows this article in the microfilm version of the journal, can be ordered from the ACS, and can be downloaded from the Internet; see any current masthead page for ordering information and Internet access instructions.

JA953976Y

(31) Zakharkin, L. I. *Izv. Akad. Nauk SSSR, Ser. Khim.* **1965**, 1114−1116.
(32) Zakharkin, L. I.; Kalinin, V. N.; Snyakin, A. P. *Zh. Obsch. Khim.* **1970**, *40*, 2424−2431.
(33) Zakharkin, L. I.; Chapovskii, Y. A. *Izv. Akad. Nauk SSSR, Ser. Khim.* **1964**, 772.
(34) Potapova, T. V.; Svitsyn, R. A.; Zhigach, A. F.; Laptev, V. T.; Persianova, I. V.; Sorokin, P. Z. *Russ. J. Inorg. Chem.* **1965**, *10*, 1133−1135.
(35) Hawthorne, M. F.; Berry, T. E.; Wegner, P. A. *J. Am. Chem. Soc.* **1965**, *87*, 4746−4750.
(36) Adler, R. G.; Hawthorne, M. F. *J. Am. Chem. Soc.* **1970**, *92*, 6174−6182.
(37) Piepgrass, K. W.; Stockman, K. E.; Sabat, M.; Grimes, R. N. *Organometallics* **1992**, *11*, 2404−2413.
(38) Zakharkin, L. I.; Stanko, V. I.; Klimova, A. I.; Chapovskii, Y. A. *Izv. Akad. Nauk SSSR, Ser. Khim.* **1963**, 2236−2237.
(39) Aleksandrov, A. Y.; Bregadze, V. I.; Gol'danskii, V. I.; Zakharkin, L. I.; Okhlobystin, O. Y.; Khrapov, V. V. *Dokl. Akad. Nauk* **1965**, *165*, 593−596.
(40) Zakharkin, L. I.; Kalinin, V. N. *Izv. Akad. Nauk. SSSR, Ser. Khim.* **1965**, 1311.
(41) Zakharkin, L. I.; Podvisotskaya, L. S. *Izv. Akad. Nauk SSSR, Ser. Khim.* **1965**, 1464−1466.
(42) Zakharkin, L. I.; Stanko, V. I.; Brattsev, V. A.; Chapovskii, Y. A.; Okhlobystin, O. Y. *Izv. Akad. Nauk SSSR, Ser. Khim.* **1963**, 2238−2239.
(43) Zakharkin, L. I.; Stanko, V. I.; Brattsev, V. A.; Chapovskii, Y. A.; Klimova, A. I.; Okhlobystin, O. Y.; Ponomarenko, A. A. *Dokl. Akad. Nauk SSSR* **1964**, *155*, 1119−1122.
(44) Zakharkin, L. I. *Dokl. Akad. Nauk SSSR* **1964**, *157*, 1149−1152.
(45) Clegg, W.; Coult, R.; Fox, M. A.; Gill, W. R.; MacBride, J. A. H.; Wade, K. *Polyhedron* **1993**, *12*, 2711−2717.
(46) Yang, X.; Knobler, C. B.; Hawthorne, M. F. *Angew. Chem., Int. Ed. Engl.* **1991**, *30*, 1507.
(47) Yang, X.; Knobler, C. B.; Zheng, Z.; Hawthorne, M. F. *J. Am. Chem. Soc.* **1994**, *116*, 7142.
(48) Grimes, R. N. *Carboranes*, 1st ed.; Academic Press: New York, 1970; p 272.
(49) Papetti, S.; Heying, T. L. *Inorg. Chem.* **1963**, *2*, 1105−1107.
(50) Papetti, S.; Schaehher, B. B.; Troscianiec, H. J.; Heying, T. L. *Inorg. Chem.* **1964**, *3*, 1444−1447.
(51) Grafstein, D.; Bobinski, J.; Dvorak, J.; Paustian, J. E.; Smith, H. F.; Karlan, S.; Vogel, C.; Fein, M. M. *Inorg. Chem.* **1963**, *2*, 1125−1126.
(52) Grafstein, D.; Bobinski, J.; Dvorak, J.; Smith, H.; Schwatrz, N.; Cohen, M. S.; Fein, M. M. *Inorg. Chem.* **1963**, *2*, 1120−1125.
(53) Heying, T. L.; Ager, J. W.; Clark, S. L.; Alexander, R. P.; Papetti, S.; Reid, J. A.; Trotz, S. I. *Inorg. Chem.* **1963**, *2*, 1097−1105.
(54) Harmon, K. M.; Harmon, A. B.; Thompson, B. C. *J. Am. Chem. Soc.* **1967**, *89*, 5309−5311.
(55) Kivekäs, R.; Sillanpää, R.; Teixidor, F.; Viñas, C.; Nuñez, R.; Mar Abad, M. *Acta Crystallogr.* **1995**, *C51*, 1864−1868.